Adiabatic shear instability is not necessary for adhesion in cold spray

As Published: 10.1016/J.ACTAMAT.2018.07.065

Publisher: Elsevier BV

Persistent URL: https://hdl.handle.net/1721.1/135807

Version: Author's final manuscript: final author's manuscript post peer review, without publisher's formatting or copy editing

Mostafa Hassani-Gangaraj, David Veysset, Victor K. Champagne, Keith A. Nelson,
Christopher A. Schuh. Acta Materialia 158 (2018) 430-439
https://doi.org/10.1016/j.actamat.2018.07.065

Adiabatic Shear Instability is Not Necessary for Adhesion in Cold Spray

Mostafa Hassani-Gangaraj[1], David Veysset[2], Victor K. Champagne[3], Keith A. Nelson[2,4], Christopher A. Schuh[1*]

[1]Department of Materials Science and Engineering, MIT, Cambridge, Massachusetts 02139, USA.

[2]Institute for Soldier Nanotechnologies, MIT, Cambridge, Massachusetts 02139, USA.

[3]U.S. Army Research Laboratory, Weapons and Materials Research Directorate, Aberdeen Proving Ground, MD, USA

[4]Department of Chemistry, MIT, Cambridge, Massachusetts 02139, USA.

[*]Correspondence to: schuh@mit.edu

Abstract

When metallic microparticles impact substrates at high enough velocity, they bond cohesively. It has been widely argued that this critical adhesion velocity is associated with the impact velocity required to induce adiabatic shear instability. Here, we argue that the large interfacial strain needed to achieve bonding does not necessarily require adiabatic shear instability to trigger. Instead, we suggest that the interaction of strong pressure waves with the free surface at the particle edges—a natural dynamic effect of a sufficiently rapid impact—can cause hydrodynamic plasticity that effects bonding, without requiring shear instability. We proceed on this basis to postulate and confirm a proportionality between critical velocity and the bulk speed of sound, which supports the viewpoint that shear instability is not the mechanism of adhesion in cold spray.

Keywords: Cold Spray, Impact, Bonding, Critical Velocity, Jetting

1. Introduction

Material build-up in cold spray revolves around the notion of impact-induced bonding of microparticles at impact velocities that exceed a threshold, referred to as the "critical velocity" [1–4]. Adiabatic shear instability [5–7], oxide layer break up [8], localized melting [9–12], diffusion [13], interface amorphization [14], and mechanical interlocking [15] are among the variety of mechanisms put forth to explain bonding. These mechanisms, although partially supported by observational data, have not been directly proven to underlie bonding yet, and are not mutually exclusive either; several of these could be relevant depending upon conditions and materials involved. Nevertheless, with critical velocity being unique for a fixed set of processing parameters and material [4–6], a predominant role of one single mechanism is expected. As such, adiabatic shear instability is the prevailing mechanism of bonding asserted in the cold spray literature [4–7,9,13,16–36].

The physical connection between adiabatic shear instability and bonding during cold spray often hangs upon the phenomenon of *jetting*, the intense outward ejection of material at the interface between particle and substrate. It is a commonly-held view in the field that adiabatic shear instability occurs on impact, leading to jetting, and it is jetting [5,19,21,37] that leads to bonding through the intense strain it produces at the interface, forming a coherent surface for bonding. The proposal of adiabatic shear instability as the cause of bonding or jetting originated about 15 years ago based on finite element simulations [5,6], and it has subsequently enjoyed support mainly from that same, simulation-based, perspective [4,7,9,13,16,20,22,24,27,29–33,35]. There is, however, a lack of empirical or experimental evidence to rigorously support the notion of adiabatic shear instability as the bonding mechanism. To the best of our knowledge, adiabatic shear bands, manifested as physical signatures of adiabatic shear instability, are rarely reported in cold sprayed particles, whereas they should be seen in each and every

of the broad range of metallic materials amenable to cold spray deposition if they were required to effect bonding.

In an effort to approach the problem of critical velocity from a different perspective, we recently experimentally resolved the instant of impact-bonding with micrometer scale and nanosecond level spatiotemporal resolution [37,38]. Through in-situ observations we confirmed that impact-induced bonding is indeed closely related to jetting, and localized fragmentation; as envisioned above, the extreme strain associated with jetting is perceived to produce a clean intimate contact amenable to metallic bonding at the interface. What is more, we reported direct measurements of critical velocity for the rebound-to-bonding transition for four structural metals [37]. Our approach offers a significant departure from prior works on this topic, and the quantitative nature of the results allows us a new view on the question of adiabatic shear instability as a mechanism for jetting and bonding. It is the purpose of this paper to revisit the nominally accepted view of adiabatic shear instability and question its viability as a general mechanism for impact adhesion. In addition to reassessing the simulated-based origin of the mechanism, we make use of our quantitative single-particle impact data to support an alternate view that jetting and bonding are a hydrodynamic plastic effect.

2. Adiabatic shear instability and jetting

We start by considering the role of adiabatic shear instability during a microparticle impact using the same framework it originated from, i.e., Lagrangian finite element simulations. The most influential simulations of particle impacts in cold spray are those based on a continuum description with constitutive behaviors that are strain-, strain rate- and temperature-dependent. Under the extreme conditions of rate and pressure relevant to supersonic particle impact, it is certainly the case that constitutive models are questionably relevant to true experimental conditions. However, the field's mechanistic knowledge has

been built on models such as the Johnson-Cook equation [39], that despite its shortcomings at very high strain rates [40,41], is the typical constitutive equation most widely used in finite element simulations of particle impact during cold spray [4–7,9,13,16,20,22,24,27,29–33,35]:

$$\sigma = \left[A + B\varepsilon_p^n\right]\left[1 + Cln\frac{\dot{\varepsilon}_p}{\dot{\varepsilon}_0}\right]\left[1 - \left(\frac{T - T_{ref}}{T_{melt} - T_{ref}}\right)^m\right] \quad (1)$$

Here the flow stress, σ, is the product of three bracketed terms. The first bracketed term represents strain hardening, with ε_p being the plastic strain, and A, B and n being material constants. The second bracketed term represents strain rate hardening, with $\dot{\varepsilon}_p$ being the strain rate, C being a material constant and $\dot{\varepsilon}_0$ being a reference strain rate. The third bracketed term represents thermal softening with T being the temperature, T_{melt} being melting temperature, m being a material constant, and T_{ref} being a reference temperature; it is this last term which gives rise to adiabatic localization, making it critical to the discussion of that mechanism.

The first and most important works on adiabatic strain instability in impact bonding are those of, first, Assadi et al. [5] and, immediately afterwards, Grujicic et al. [6] , who implemented Eq. 1 in a Lagrangian finite element model to simulate the behavior of a Cu particle impacting a Cu substrate at the critical velocity. As a means of connecting with those classic works, we have implemented the same mechanics in a similar Lagrangian finite element framework in order to duplicate their approach, and simulated the behavior of a single Cu particle at 550 m/s, representing our directly measured critical velocity of Cu, 553±15 m/s, in Ref. [37]. More details of our finite element model are collected in Appendix A.

Figure 1a shows snapshots of a 10-µm Cu particle impacting Cu at the critical velocity. Critically, this result includes important contributions from all the three bracketed terms of the constitutive equation, i.e., with competing hardening (first two strain and rate hardening terms) and softening behaviors (thermal softening from the third term). As expected based on the work of refs. [5,6], incipient jetting is observed

at the periphery of the particle. In fact, the lip forming at the particle edge is a similar size and shape seen in the similar simulations of ref. [5], as shown by the comparison in Fig. 1a.

The beginning of jet formation seen in Fig. 1a has been interpreted in refs. [5,6] as being caused by heat induced by severe and rapid plastic deformation (note that the strain here is as high as 4.5 in the forming jet, and forms over 25 ns or less). This adiabatic heat is assumed to locally soften the material to the point where it loses its load-bearing capacity, thus, jetting has been taken to occur as a result of adiabatic shear instability [4–7,9,16–30,33–36]. Thus, the third bracketed term in the constitutive law of Eq. 1 is the key term that physically supports an argument for adiabatic shear instability; it is the only term that provides the material with the ability to soften.

A critical test of this mechanism, then, is to verify that jet or lip formation is suppressed if the material has no softening capacity. We have excluded the thermal softening term from Eq. 1, and repeated the same simulation in every other detail; we eliminated the material's ability to thermally soften, and by extension to experience an adiabatic shear instability. Fig. 1b shows snapshots of deformation for a material that only hardens as it deforms. It is interesting to observe that jetting occurs in this latter case too, with the results being almost identical in details of the strain distribution, the flattening of the particle, etc. We do see that the jet region is slightly more extended in the former case where thermal softening contributes to the deformation. Thus, thermal softening clearly can affect material deformation and failure, especially in the jet region after it has begun to form. However, this comparative modeling result shows that thermal softening, and by extension, adiabatic shear instability, is not fundamentally needed for jetting. We therefore find the conclusion drawn in the original modeling work of Assadi et al. [5] and Grujicic et al. [6], "bonding can be attributed to adiabatic shear instabilities which occur at the particle surface at or beyond the critical velocity", to be overstated, and we therefore now proceed to consider in more detail the phenomenon of jet formation.

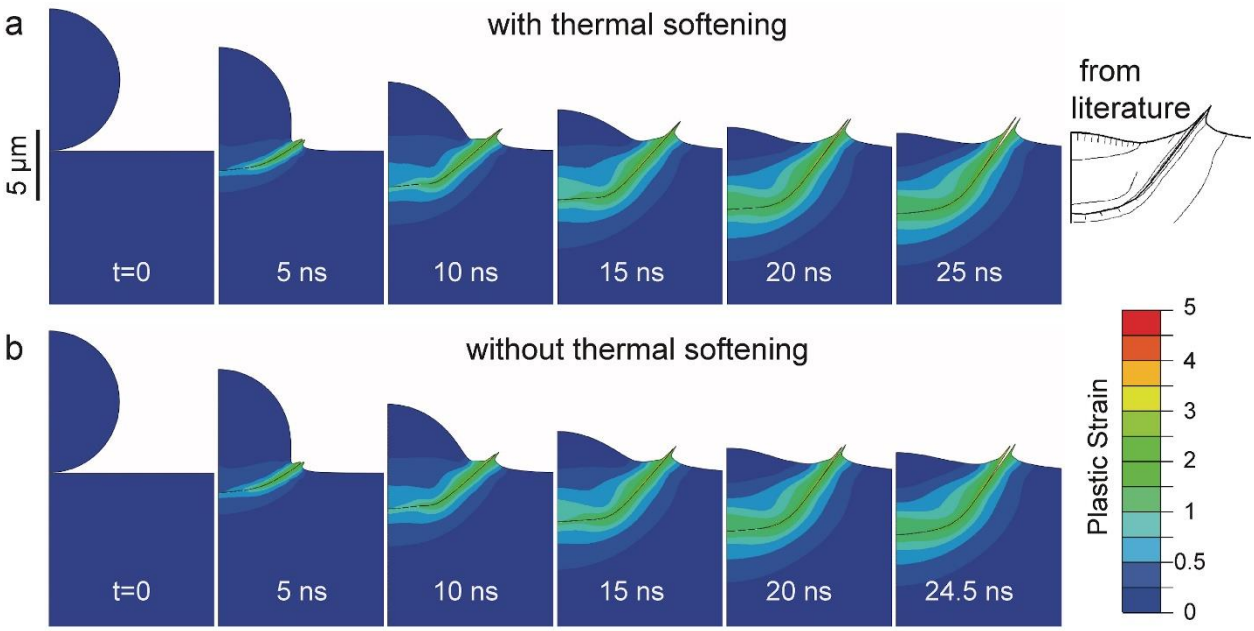

Fig. 1. Lagrangian finite element simulation of a 10-µm Cu particle impacting a Cu substrate at 550 m/s, the critical velocity of Cu. von Mises Plastic strain distribution and snapshots of deformation until the end of penetration are shown for **a)** a material with the thermal softening capability in the constitutive equation and **b)** a material without the thermal softening capability, hence, without the ability to undergo adiabatic shear instability. Jetting is observed in both cases. For comparison, the black and white image is a scaled reproduction of the results for a Cu particle/substrate pair after impact at 600 m/s from ref. [5], reproduced with permission from Elsevier.

Since jetting plays a critical role for bonding in cold spray, accurate quantitative knowledge of material conditions in the jet region is certainly needed. For example, the present Lagrangian simulation shows that von Mises strain in the jet region can be locally as high as 450%. It is a serious concern that this high plastic strain occurs only in a few elements that undergo an extreme level of distortion (by a factor of as much as 100), and this is a principal criticism of Lagrangian simulations of such a process, which do not yield highly accurate estimates of strain, stress, or temperature in the jet region [42].

One approach to avoid such extreme distortion and thereby more accurately estimate the material conditions that prevail in the forming jet, is to employ an Eulerian approach where material flows through stationary elements [42]. The induced pressure in supersonic impact of metallic particles can greatly

exceed the yield stress of the material. In such conditions, where the fractional deviations from stress isotropy are small, solid materials behave hydrodynamically, conditions for which an Eulerian formulation has proven more effective than a Lagrangian one [43]. And, since sliding cannot be accurately modeled when two Eulerian objects come into contact [44–49], we use a coupled Eulerian-Lagrangian approach [50–52], in which a Lagrangian substrate is used only to provide an appropriate platform for the deformation of the Eulerian particle. Again, more details are provided in Appendix A.

Repeating the same simulation conditions in this new framework (for a Cu particle impacting a Cu substrate at 550 m/s) yields the result shown in Fig. 2, where different element resolutions of the Eulerian domain are compared. The Eulerian approach permits fragmentation and surface creation without needing explicit interface-tracking, and can therefore capture jetting and material ejection when it is mechanically favored [43]. It can be seen that the overall deformation of the bulk of the particle is not highly mesh-dependent, whereas the material behavior in the jet region is. Our results suggest that a mesh resolution of *d/50* or finer (with *d* the particle diameter) is needed to capture jetting and fragmentation at the critical velocity. In analogy with Fig. 1a vs. 1b, Figs. 2a and 2b also verify that actively excluding thermal softening does not suppress jetting. The exclusion of softening results in slightly less severe deformation in the jet, but in these more refined Eulerian simulations, too, jetting happens with or without the material having thermal softening capacity.

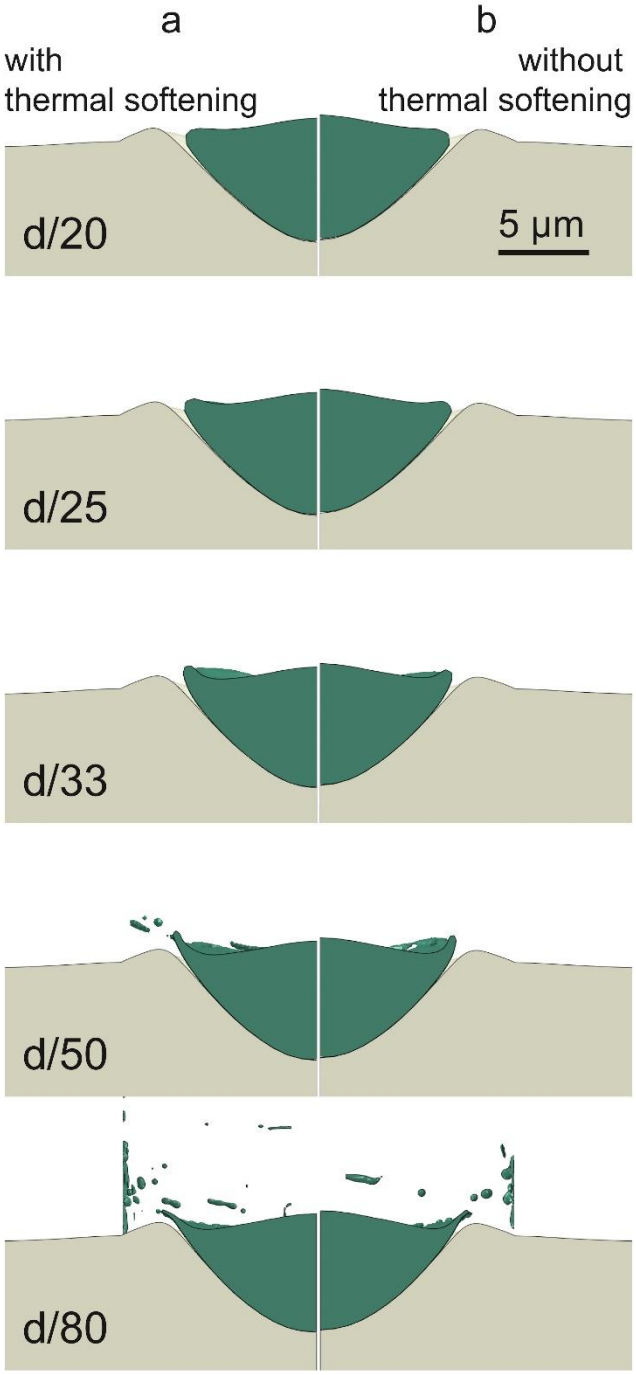

Fig. 2. Final deformation of a Cu particle impacting a Cu substrate at the critical velocity of Cu, 550 m/s, for different Eulerian mesh resolutions **a)** with and **b)** without thermal softening capacity. Penetration ends after 25 and 24 ns for **a** and **b** respectively. Although the bulk of the deformation can be captured with a coarse d/20 resolution, resolutions finer than d/50 are needed to capture jetting and fragmentation. Note that in the d/80 simulation the ejecta reach the edge of the simulation cell and aggregate unphysically against the boundary there. However, the Lagrangian substrate does not interact with the Eulerian boundary, so the alignment of the pile-up extent with this edge is coincidental.

3. What causes jetting if not adiabatic shear instability?

The avoidance of mesh distortion in the Eulerian particle of Fig. 2 permits us to look in more detail at the conditions that prevail in the jet region, provided we use the most relevant physical model for material behavior. For all of the simulations that follow, we employ the full Johnson-Cook model, inclusive of thermal softening, with the aim of better understanding the conditions in the forming jet. Figure 3 shows snapshots of a Cu particle deforming as a result of impact at critical velocity, along with the pressure distribution. Here we demonstrate relatively high pressures with red, intermediate pressures with yellow, relatively high tensions with blue and intermediate tensions with cyan. In the early stages of impact, a highly compressed state of matter (shock) is formed at the contact zone—from the impact center to the contact edge—a region that is extremely small at first contact and which expands as the impact develops and the particle flattens to create more interfacial area. The shock front remains attached to the expanding edge of the particle at the early stage [53,54]. We have recorded a maximum pressure of ~14 GPa at this stage.

The contact edge outward velocity is initially higher than the shock wave velocity. However, it decreases with time, enabling the pressure waves to detach from the particle's edge (see 2.5 ns). At this stage the high-pressure zone is immediately adjacent to the free surface where the pressure is necessarily zero. A very large pressure gradient is, therefore, created in the immediate vicinity of the free surface. Material subjected to this pressure gradient accelerates, releasing the pressure and undergoing a localized tension to form a small incipient jet 'lip' (see 3.4 ns). In the meantime the pressure waves reach the top surface of the particle and get released there, exposing a larger area on the top to a relatively higher tension, ~ 1 GPa.

These two pressure releases are different. The latter (at the top of the particle) is the result of the interaction of pressure waves and free surface that are moving in opposite directions. Even though it

produces a relatively larger tension, it gets immediately released; it lasts for less than a nanosecond. This is the interaction that causes deceleration of the top of the particle. The former (at the edge of the contact), on the other hand, is the result of the interaction of pressure waves and free surface that are moving *in the same* direction. It produces a large degree of tension that can be as high as five times the strength of Cu. This pressure release thus further accelerates material in the form of a jet, and it lasts much longer. In fact, it lasts until the end of the deformation; see the jet region in cyan out until 25 ns in Fig. 3. It is this state of hydrodynamic tension in the jet region that can lead to localized fragmentation in a spall-like process [55,56] as observed in-situ in ref. [37].

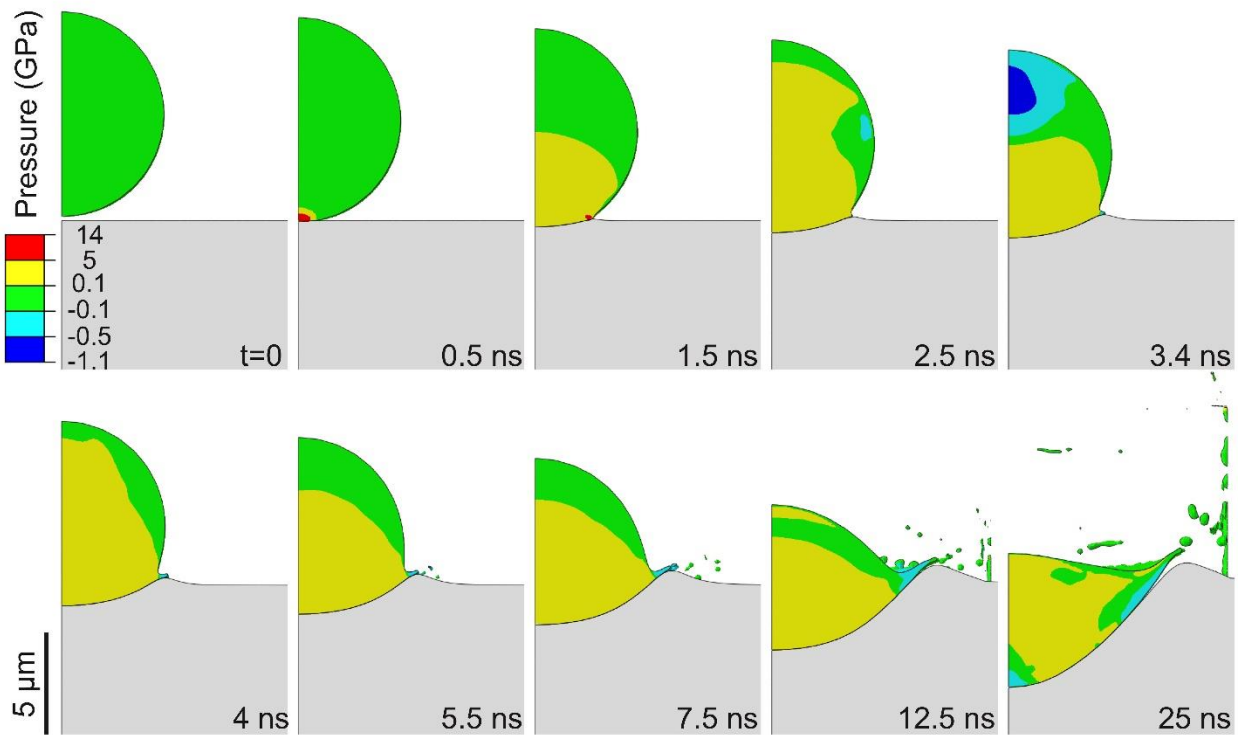

Fig. 3. Deformation and pressure distribution for a Cu particle impacting a Cu substrate at the critical velocity, 550 m/s. The particle that is initially 200 nm away touches the substrate at 0.36 ns. The particle fully penetrates the substrate after 25 ns. Red and yellow show relatively high and intermediate pressures. Blue and cyan show relatively high and intermediate tension. Green, with 0±0.1 GPa pressures represents either uncompressed material or the transition between tension and compression. Note the initial yield

strength of Cu is ~0.1 GPa, and these simulations use all of the terms of the Johnson-Cook model, including the softening term.

We thus argue that jetting occurs on the basis of a pressure release at the particle edge (Fig. 3), and schematically summarize our modeling results in Fig. 4 where the three stages of jetting, from impact-induced shock to shock detachment and to jet formation, are presented. Jetting happens whether or not the material is capable of adiabatic softening (Fig. 2) because the hydrodynamic stresses are so high as to easily exceed the flow strength of the material. To the extent that jetting is the critical phenomenon enabling solid-state bonding, we argue that bonding does not require adiabatic shear instability and hydrostatic pressure release can play its putative role instead.

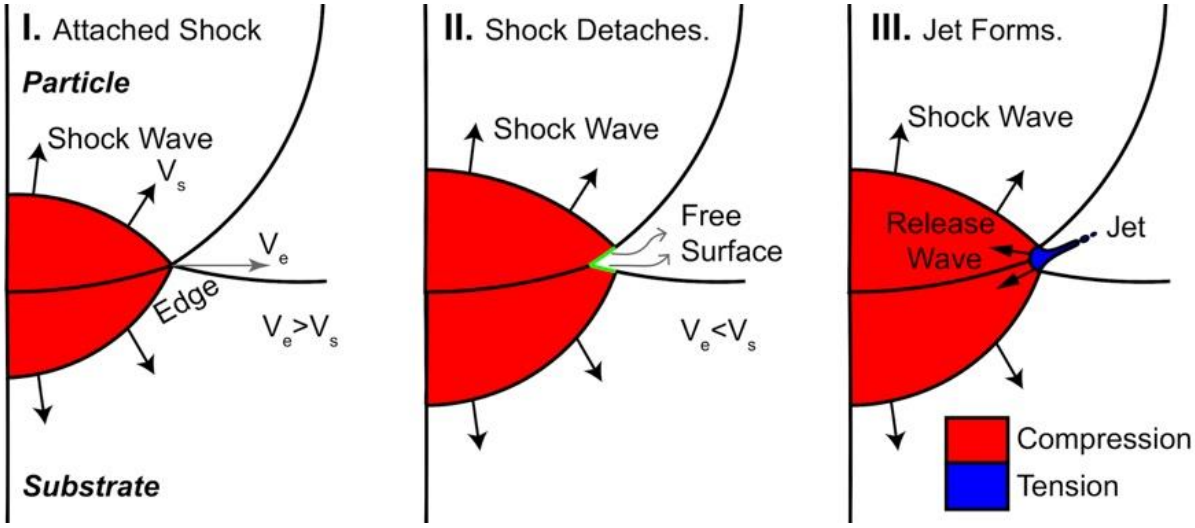

Fig. 4. Schematic representation of jetting in cold spray: **Stage I.** Impact induces a shock wave. **Stage II.** Shock detaches form the leading edge. **Stage III.** Jet forms on the basis of pressure releases. Note: the uniformity of the colors is not meant to suggest that pressure/tension is uniformly distributed.

Based on the schematic representation in Fig. 4, one can estimate the time at which jetting is triggered by estimating and equating the contact edge velocity (V_e) and the shock velocity. We make a first order approximation of the contact edge velocity at the early stage of matched materials impact based on the conservation of volume by $V_e = [V_i(d - V_i t)] \Big/ \left[4\sqrt{\frac{V_i t}{2}(d - \frac{V_i t}{2})}\right]$, where V_i is the impact velocity, d is the particle diameter, and t is time. This equation is derived based on a geometrical relation between the penetration, contact radius and particle dimeter and its differentiation with respect to time. We neglect the deceleration of the interface at the early stage when the pressure and the inertial effects dominate the deviatoric stresses, and take the interface velocity to be the interface velocity at the beginning of contact in matched materials impact, i.e., $V_i/2$. Next, we can calculate the shock velocity in the early stage of the matched materials impact using the Hugoniot relation [57], $V_s = C_0 + s\,V_i/2$ where C_0 is the bulk speed of sound, and s is a material constant empirically determined.

Based on the pressure-release mechanism, jetting is possible when the edge velocity drops below the shock velocity, i.e., $V_e < V_s$. Setting the above expressions for these two velocities equal and solving thus provides an estimate of the conditions where jetting can happen. While the parameters that go into such an analysis can be varied over broad ranges, we can take the approach of physically bounding the discussion using reasonable extreme values of the inputs. For example, given that the critical velocities and particle diameters relevant to cold spray are in the range of 250-1000 m/s and 10-100 µm [2] we can evaluate bounds on V_e. This is shown in Fig. 5, where we construct upper and lower bounds for V_e by applying 1000 m/s for V_i and 10 µm for d, and 250 m/s for V_i and 100 µm for d, respectively. We also construct upper and lower bounds for the shock wave velocity by constraining C_0 and s to reasonable limiting values for metallic materials, i.e., using C_0 = 6000 m/s , V_i = 1000 m/s , and s = 2, and C_0 = 3000 m/s, V_i = 250 m/s, and s = 1 respectively.

The crossover between these various bounds is shown by the overlapped shaded regions in Fig. 5; we view the twice-shaded region as providing a plausible time range when the shock wave detaches from the leading edge; solutions outside this region require input values beyond the reasonable limits described above. More specifically, the shock wave detachment from the contact edge, as a result of which a jet may form, has an upper bound time on the order of ~1 ns. Jetting is thus expect to occur in the very early stages of deformation when compared to the typical contact time in cold spray, which considering the above-mentioned bounding velocities and particle diameters, can be in the range of d/V_i = 10-400 ns.

From Lagrangian simulations in the literature, adiabatic shear localization was reported to occur 30 ns after impact of a 10-µm copper particle onto a copper substrate by Assadi et al. [5], after 12 ns for a 25-µm copper particle by Grujicic et al. [6], after 40 ns for a 25-µm copper particle [7] and after ~20 ns for Al6061 [29]. Thus, when Lagrangian simulations have identified jetting and attributed it to shear localization, it usually occurs at later times of the order ~10-40 ns. Related recent microstructural characterizations of adiabatic shear bands [58] also point toward the gradual character of that phenomenon, suggesting that it can be described as a nucleation and growth failure mechanism that evolves over a duration of time. Our results in Fig. 3, on the other hand, show that the pressure wave is already interacting with the leading edge at 0.5 ns, and that material is already ejecting out to form an incipient jetting lip at the snapshot taken at 2.5 ns, a time scale that matches the pressure-release basis for jet formation in Fig. 5.

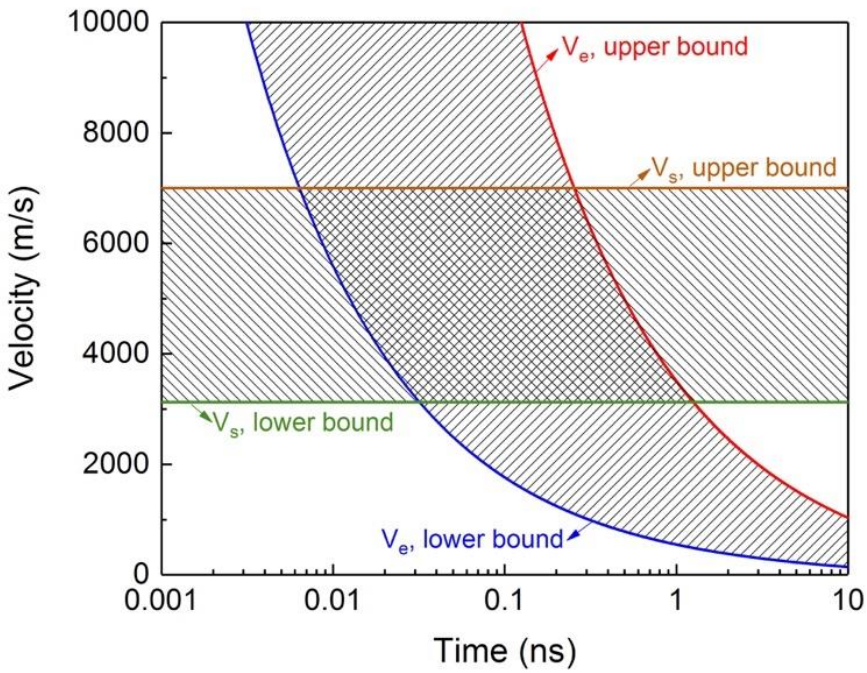

Fig. 5. Upper and lower bound velocities for the particle contact edge and the pressure wave relevant to cold spray conditions. Our analysis shows that the upper bound on time for the shock wave to detach form the leading edge, a mechanism that can give rise to jetting, is on the order of ~1 ns in metallic microparticle impact.

It is important to note that the material in the jet region, once it forms due to this hydrodynamic mechanism, is experiencing a large amount of very rapid plastic deformation. Figure 6a shows the von Mises plastic strain distribution as the particle deforms following impact at the critical velocity. Plastic deformation is localized at the interface, and adiabatic temperature rise can (and does) result, as shown in the accompanying snapshots of Fig. 6b. The temperature at the particle edge when the jet is about to form is between 500 and 600 K. As a result of such temperature rise, the material can soften below its original strength. However, in this particular simulation such strength loss is not found for any material not ejected. In fact, stress conditions shown in Fig. 7 are far from the threshold expected to trigger

autocatalytic localization. Thus, with the present results on Cu, we do not rule out the possibility of adiabatic shear instability occurring *as a result (but not a cause)* of jet formation, especially for materials with much lower thermal diffusivities than that of Cu. We can thus reconcile the expectation that impact should indeed lead to significant temperature rise (it does) with the fact that this need not lead to adiabatic shear instability (it need not); jetting will happen independently due to the hydrodynamic pressure release mechanism.

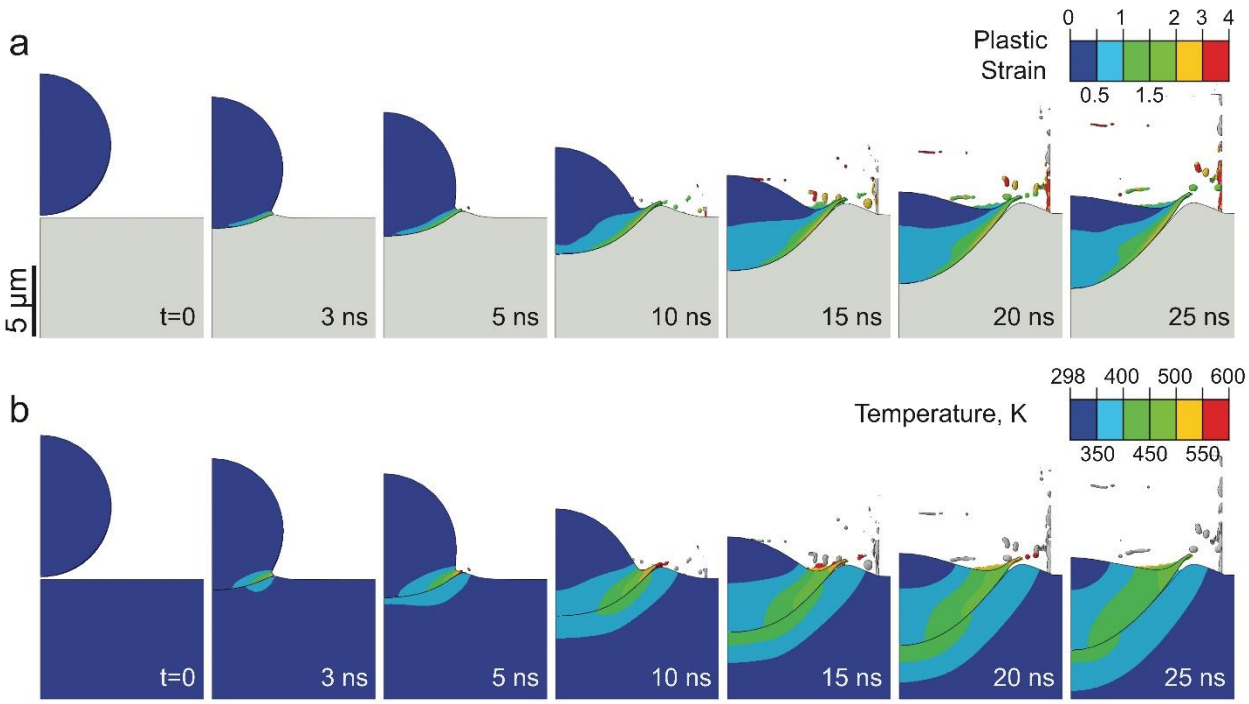

Fig. 6. Temporal and spatial evolution of **a)** von Mises plastic strain and **b)** temperature as a Cu particle impacting a Cu substrate deforms at the critical velocity. These simulations use the full Johnson-Cook model, inclusive of the thermal softening term. Note again that in the later frames of these sequences the ejected jet material is unphysically piled against the edge of the Eulerian simulation cell and should be disregarded.

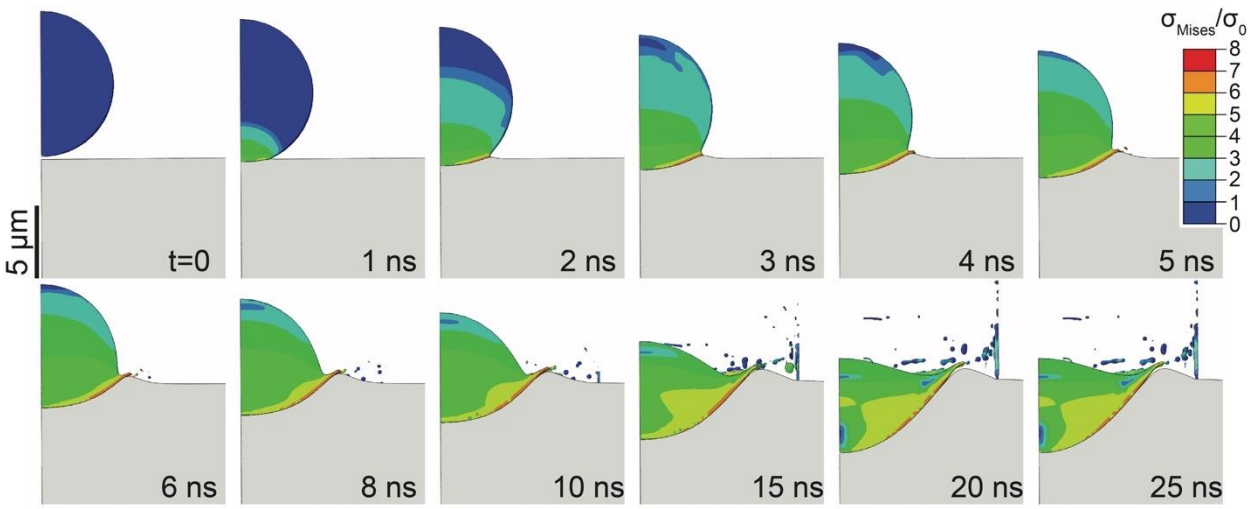

Fig. 7. Temporal and spatial evolution of Mises stress (instantaneous flow stress) normalized by the initial flow stress as a Cu particle impacting a Cu substrate deforms at the critical velocity. Note that these simulations involve the full Johnson-Cook model, including the thermal softening term.

As final note in this section, we observe that an analogy between jetting in cold spray and jetting in other areas such as explosive welding [59,60], micro-droplet impact [53,54], shaped charges [61,62], and asteroid strikes [63,64] is plausible (see Fig. 8 a-d). Among these, explosive welding is in principal very similar to cold spray, as solid-state bonding results in both cases after jetting sets on [65,66]. In all the areas of research in Fig. 8, jetting has been documented, discussed, and understood as hydrodynamic phenomenon related to pressure release after impact. Whereas the importance of hydrodynamic effects is underrepresented in the field of cold spray— except for a few works, ref. [67] for instance—from the above analogy, it is reasonable to consider that material jetting in cold spray (Fig. 8e), too, can occur on the basis of pressure release rather than on the basis of adiabatic shear instability.

Mostafa Hassani-Gangaraj, David Veysset, Victor K. Champagne, Keith A. Nelson, Christopher A. Schuh. Acta Materialia 158 (2018) 430-439
https://doi.org/10.1016/j.actamat.2018.07.065

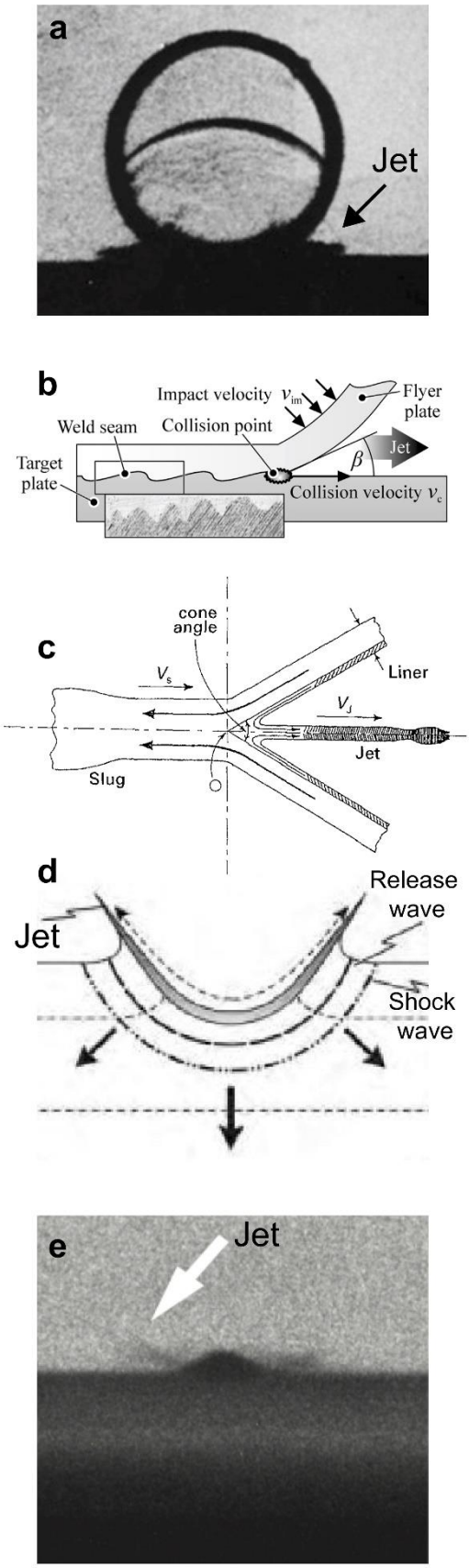

Fig. 8 Jetting and material ejection during impact of converging geometries in different fields from **a)** droplet impact, to **b)** explosion welding, to **c)** shaped-charges, to **d)** meteorite impact are discussed as a hydrodynamic phenomenon. The same can explain jetting in **e)** microparticle impact. Images are taken form refs [37,61,68–70] , reproduced with permission from Elsevier, Springer Nature, and John Wiley and Sons.

4. Mechanistic Argument

Our finite element model suggests that pressure release is the origin of jetting in microparticle impact. Increasing impact velocity results in higher impact-induced pressures which in-turn results in higher reflected tensions. When the transient state of hydrodynamic tension exceeds the material dynamic strength, a process of spall occurs. Given the geometry at the contact, this would be observed as an unstable ejection of material in form of a jet and subsequent fragments. While this argument justifies the existence of a threshold velocity for jetting, a knowledge of the induced tension and the dynamic strength would be required in order to estimate the threshold impact velocity for such localized unstable jetting. In what follows we develop a first-order approximation of the critical velocity for jetting by estimating and equating the two. First, it is reasonable to assume that the amplitude of the induced tension after pressure release is proportional to its source, i.e., the impact-induced pressure:

$$P^{-} = k \times \frac{1}{2}(\rho C_0 V_i + s\frac{\rho V_i^2}{2}) \tag{2}$$

with P^{-} being the amplitude of the induced tension, ρ the density, C_0 the bulk speed of sound, V_i impact velocity, and s a material constant. The parameter k captures the assumed proportionality between impact pressure and induced tension.

Second, inspired by the observation of discernible isolated ejecta in our in-situ experiments [37], as a first step, we propose that spall strength [55,56] can reasonably represent material strength against shock-induced localized fragmentation in microparticle impact. From first principles, spall strength is

proportional to the bulk modulus for pure metals. The proportionality constant is, generally, a function of temperature and strain rate:

$$P_s = \alpha \times \beta(T, \dot{\varepsilon}) \times B = \alpha \times f(T) \times h(\dot{\varepsilon}) \times B \tag{3}$$

Where B is the bulk modulus, and $f(T)$ and $h(\dot{\varepsilon})$ are coefficients that represent the temperature and strain rate dependency of the spall strength. We note that the latter function can also be approximated as a function of size, $g(d)$, given that the cold spray critical velocity is on the order of ~100 m/s. α is a constant that can be estimated from models such as Orowan's sinusoidal interatomic potential [71] or the Morse potential [55], or fitted to spall strength measurements of pure metals [72]; the latter approach suggests a best-fit value of ~1/150 [72].

Equating (2) and (3) yields a quadratic equation for the threshold impact velocity, V_{cr}, required to trigger material ejection and fragmentation. Of the two roots of this equation, one is negative and non-physical. The positive root gives a first order approximation of the critical velocity:

$$V_{cr} = \left(\frac{\sqrt{1 + \frac{4s\alpha f(T) g(d)}{k}} - 1}{s} \right) \times \sqrt{\frac{B}{\rho}} \approx \frac{2\alpha f(T) g(d)}{k} \times \sqrt{\frac{B}{\rho}} \tag{4}$$

This expression linearly relates the critical impact velocity to the bulk speed of sound, $C_0 = \sqrt{\frac{B}{\rho}}$, for pure metals; note that the phenomenon is not predicted to be governed by heat transfer or thermal softening as in the shear localization mechanism, but is instead governed by elastic properties, which control the timescale of shock/pressure propagation in the material. As noted above, it is a tacit assumption in the

field (which we continue to make here) that such jetting and the attendant large interfacial strain it involves produce a clean metallic contact capable of bonding, and thus that V_{cr} is effectively equal to the critical velocity for cold spray bonding. Thus, Eq. (4) is taken as a prediction of critical adhesion velocity, and now provides a crucial test that can differentiate between the present proposal and the adiabatic shear localization mechanism widely discussed in the literature: the hydrodynamic mechanism expects linear dependence on the speed of sound.

Since α and s are constants, we can verify the proposed proportionality between the critical velocity and the bulk speed of sound by fixing temperature and particle size and measuring the critical velocity. To do so, we revisit our real-time measurements of critical velocity for 10-15 µm particles of Al, Cu, Ni, and Zn at room temperature from Ref. [37]. Those metals' critical velocities are presented as a function of their respective bulk speeds of sound in Fig. 9, and lie convincingly on a linear trend-line that intersects the origin, exactly as expected from Eq. 4.

Considering the range of physical, thermal and mechanical properties that are spanned by these different metals, we find this alignment to be noteworthy. Note, for instance, that these points are arranged in a fashion that is non-monotonic with respect to the metals' melting temperatures (Zn < Al < Cu < Ni), shear strengths or moduli (Al < Zn < Cu < Ni), densities (Al < Zn < Ni < Cu), etc. Although many mechanisms have been advanced to explain impact induced adhesion, the experimental collapse of these four very different metals onto a single trendline associated with their bulk speed of sound is a strong indicator that the pressure wave, and its interaction with the particle edge, is a dominant factor in jet formation and bonding.

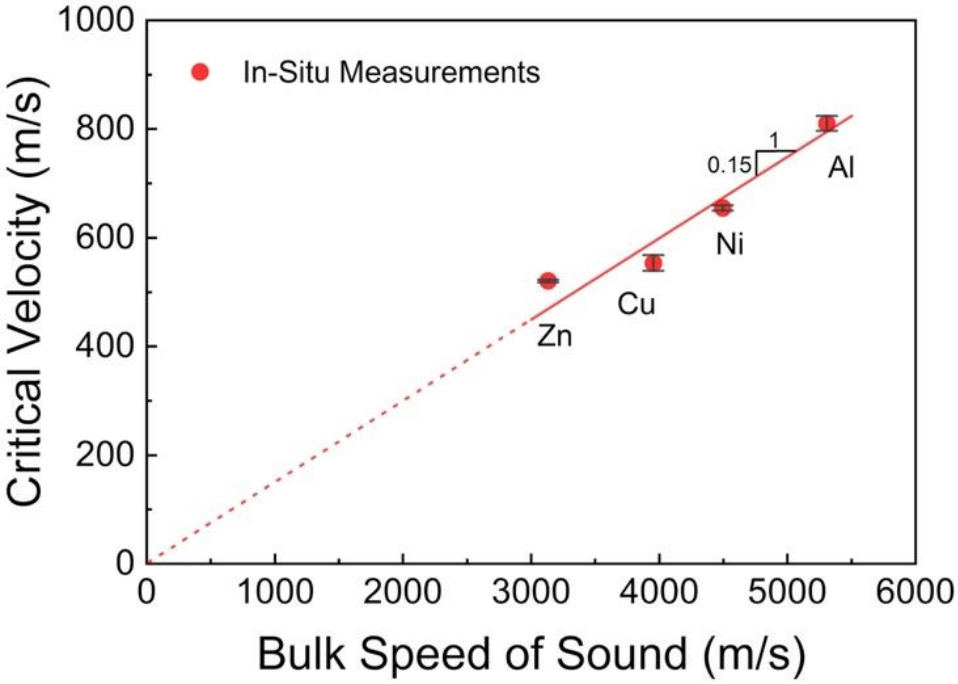

Fig. 9. In-situ measurements of critical velocity when plotted versus bulk speed of sound confirms the proportionality suggested by Eq. 4. The slope for ~10-µm particles impacting matched material substrates at room temperature is 0.15. Critical velocities were taken from ref. [37].

5. Conclusions and Outlook

This paper suggests that in a process of microparticle impact, such as in cold spray, adhesion is not fundamentally connected to a process of shear localization, as widely believed in the literature. By revisiting the same modeling framework previously used in the literature to support the prominent role of adiabatic shear instability in jet formation, we show that adiabatic softening is not needed to see the onset of jetting. Specifically, we removed the thermal softening capacity of material from the constitutive behavior and yet observed jetting at the critical velocity.

Instead, we propose that jetting in cold spray is formed as a result of strong pressure waves interacting with the expanding edge of the particle; material in the jet region is prone to localized fragmentation

under a spall-like process. A survey of other hydrodynamic processes such as liquid droplet impact, shaped-charge jetting, and explosion welding provided a variety of analogous situations in which hydrodynamic jetting occurs. The hydrodynamic jetting mechanism is primarily a pressure-driven phenomenon, and led us to develop physical support for a proportionality between the cold spray critical velocity and the bulk speed of sound. We verified this proportionality with our direct measurements of the critical velocity. These results provide a new mechanistic view for the process of impact-jetting and adhesion in cold spray.

With Eq. 4 capturing the essential materials-physics aspects of critical velocity in impact-induced bonding, we foresee that it can be extended to more complicated forms to include e.g. specific size effects, particle temperature effects, native oxide thickness effects, impact angle effects, and materials strength effects, as our proposed mechanistic picture is likely to need adaptation to address all these. While we leave the detailed extension of Eq. 4 to future studies, we note that the simplest version of it in the form of a proportionality to the bulk speed of sound, is useful to emphasize the nature of impact jetting and critical velocity as being fundamentally pressure driven.

Acknowledgement

This research was accomplished through a cooperative research agreement with the US Army Research Laboratory, Contract: W911NF-15-2-0034, **"**Development of Additive Manufacturing and Advanced Materials Processing for the DOD".

Appendix A: Finite Element Models

Lagrangian Model

Using ABAQUS 6.14-3 [73], we developed an axisymmetric coupled thermo-mechanical dynamic explicit model to simulate the high-velocity-impact behavior of a 10-µm Cu particle onto a Cu substrate. We chose Cu since it is the popular material of choice in numerical studies of cold spray impacts. We modeled the substrates to be the cross section of a cylinder with 100-µm diameter and 50-µm height (Fig. A1a).

We used 4-node thermally coupled axisymmetric quadrilateral, bilinear displacement and temperature elements with reduced integration and hourglass control to discretize the particle and the substrate. We used a *d/30* mesh resolution to have our simulations as similar as possible to what is typically seen in prior literature. Interface contact elements were introduced using the penalty algorithm with a Coulomb friction coefficient of 0.2. The substrate's bottom was constrained against all degrees of freedom, and the initial temperature of the particle and the substrate was set to 298 K. The initial particle velocity of the particle was set to 550 m/s, which is the directly measured critical velocity of a 10-µm Cu particle when impacting a Cu substrate.

Coupled Eulerian- Lagrangian Model

We also developed a three dimensional coupled thermo-mechanical dynamic explicit model to simulate the high-velocity-impact behavior of a 10-µm Cu particle onto a Cu substrate. We considered the Eulerian domain to be a stationary cuboid of 10×10×18 μm^3 in order to represent possible positions of the particle material's flow. A scalar parameter, namely volume fraction, was assigned to each element such that the model represents a quarter-sphere at the beginning of the analysis (Fig. A1b). As the material flows through the Eulerian elements, the local volume fraction is computed and the material boundary is updated. 8-node thermally coupled linear Eulerian brick elements with reduced integration and hourglass

control were used to discretize the Eulerian domain. We considered the substrate to be a quarter cylinder of the same material as the particle, with 80 µm diameter and 40 µm height. We discretized the substrate using Lagrangian elements. Normal velocities were set to zero for all six faces of the Eulerian domain to prevent material loss. We applied a symmetry boundary condition to the substrate lateral faces (normal displacement was set to zero), and constrained the substrate bottom against all degrees of freedom. The initial temperature of the particle and the substrate was set to 298 K. The initial particle velocity was set to 550 m/s which is our directly measured critical velocity of a Cu particle when impacting a Cu substrate.

Material Behavior

To capture the elastic and plastic response of Cu we used the Mie-Grüneisen equation of state [57] and the Johnson-Cook equation [39] in our coupled thermomechanical simulations. Table A1 summarizes the physical, thermal, and mechanical parameters [39,57,74] for Cu used in the simulations.

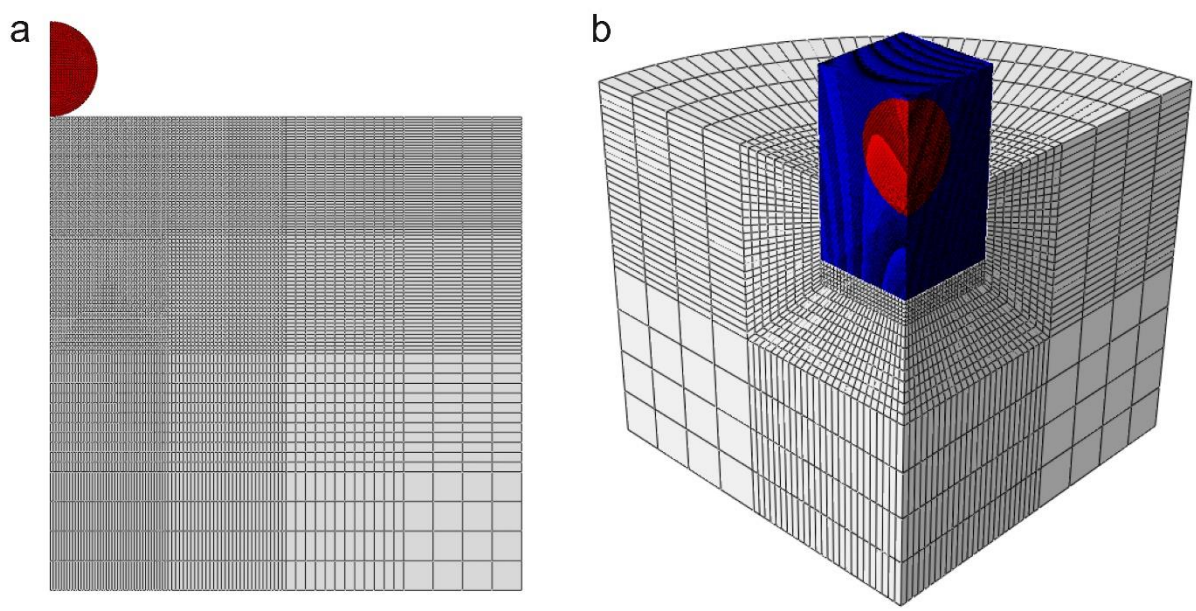

Fig. A1. Finite element model of **a)** Lagrangian particle impacting Lagrangian substrate and **b)** Eulerian particle impacting Lagrangian substrate. Particle diameter in both models is 10 µm.

Table A1. Physical, thermal and mechanical parameters of Cu used in the simulation.

Density (kg/m^3)	8960
Specific heat (J/kg K)	384.6
Melting temperature (K)	1357
Heat of Fusion (kJ/kg)	208.7
Conductivity (W/m K)	401
Shear Modulus (GPa)	48
Poisson's ratio	0.34
Bulk Modulus (GPa)	140
C_0 (m/s)	3952.8
s	1.49
Grüneisen Parameter	2.01
A (MPa)	90
B (MPa)	292
n	0.31
C	0.025
m	1.09
$\dot{\varepsilon}_0$ (s^{-1})	1
T_{ref} (K)	298

Mostafa Hassani-Gangaraj, David Veysset, Victor K. Champagne, Keith A. Nelson, Christopher A. Schuh. Acta Materialia 158 (2018) 430-439
https://doi.org/10.1016/j.actamat.2018.07.065

References

[1] H. Assadi, H. Kreye, F. Gärtner, T. Klassen, Cold spraying – A materials perspective, Acta Mater. 116 (2016) 382–407. doi:http://dx.doi.org/10.1016/j.actamat.2016.06.034.

[2] A. Moridi, S.M. Hassani-Gangaraj, M. Guagliano, M. Dao, Cold spray coating: review of material systems and future perspectives, Surf. Eng. 30 (2014) 369–395. doi:10.1179/1743294414Y.0000000270.

[3] A. Papyrin, V. Kosarev, S. Klinkov, A. Alkhimov, V.M. Fomin, Cold Spray Technology, Elsevier Science, 2006. https://books.google.com/books?id=XjZMWNVvgLAC.

[4] T. Schmidt, F. Gärtner, H. Assadi, H. Kreye, Development of a generalized parameter window for cold spray deposition, Acta Mater. 54 (2006) 729–742. doi:10.1016/j.actamat.2005.10.005.

[5] H. Assadi, F. Gärtner, T. Stoltenhoff, H. Kreye, Bonding mechanism in cold gas spraying, Acta Mater. 51 (2003) 4379–4394. doi:10.1016/S1359-6454(03)00274-X.

[6] M. Grujicic, C.L. Zhao, W.S. DeRosset, D. Helfritch, Adiabatic shear instability based mechanism for particles/substrate bonding in the cold-gas dynamic-spray process, Mater. Des. 25 (2004) 681–688. doi:10.1016/j.matdes.2004.03.008.

[7] G. Bae, Y. Xiong, S. Kumar, K. Kang, C. Lee, General aspects of interface bonding in kinetic sprayed coatings, Acta Mater. 56 (2008) 4858–4868. doi:10.1016/j.actamat.2008.06.003.

[8] W.-Y. Li, C.-J. Li, H. Liao, Significant influence of particle surface oxidation on deposition efficiency, interface microstructure and adhesive strength of cold-sprayed copper coatings, Appl. Surf. Sci. 256 (2010) 4953–4958. doi:10.1016/j.apsusc.2010.03.008.

[9] G. Bae, S. Kumar, S. Yoon, K. Kang, H. Na, H.-J. Kim, C. Lee, Bonding features and associated mechanisms in kinetic sprayed titanium coatings, Acta Mater. 57 (2009) 5654–5666. doi:10.1016/j.actamat.2009.07.061.

[10] M. Grujicic, J.R. Saylor, D.E. Beasley, W.S. DeRosset, D. Helfritch, Computational analysis of the interfacial bonding between feed-powder particles and the substrate in the cold-gas dynamic-spray process, Appl. Surf. Sci. 219 (2003) 211–227. doi:10.1016/S0169-4332(03)00643-3.

[11] W.-Y. Li, C. Zhang, X. Guo, C.-J. Li, H. Liao, C. Coddet, Study on impact fusion at particle interfaces and its effect on coating microstructure in cold spraying, Appl. Surf. Sci. 254 (2007) 517–526. doi:10.1016/j.apsusc.2007.06.026.

[12] C.-J. Li, W.-Y. Li, Y.-Y. Wang, Formation of metastable phases in cold-sprayed soft metallic deposit, Surf. Coatings Technol. 198 (2005) 469–473. doi:http://dx.doi.org/10.1016/j.surfcoat.2004.10.063.

[13] S. Guetta, M.H. Berger, F. Borit, V. Guipont, M. Jeandin, M. Boustie, Y. Ichikawa, K. Sakaguchi, K. Ogawa, Influence of Particle Velocity on Adhesion of Cold-Sprayed Splats, J. Therm. Spray Technol. 18 (2009) 331–342. doi:10.1007/s11666-009-9327-0.

[14] K.H. Ko, J.O. Choi, H. Lee, The interfacial restructuring to amorphous: A new adhesion mechanism of cold-sprayed coatings, Mater. Lett. 175 (2016) 13–15. doi:10.1016/j.matlet.2016.03.132.

[15] V.K. Champagne, M.K. West, M. Reza Rokni, T. Curtis, V. Champagne, B. McNally, Joining of Cast ZE41A Mg to Wrought 6061 Al by the Cold Spray Process and Friction Stir Welding, J. Therm. Spray Technol. 25 (2016) 143–159. doi:10.1007/s11666-015-0301-8.

[16] G. Bae, J. Jang, C. Lee, Correlation of particle impact conditions with bonding, nanocrystal formation and mechanical properties in kinetic sprayed nickel, Acta Mater. 60 (2012) 3524–3535. doi:https://doi.org/10.1016/j.actamat.2012.03.001.

[17] T. Hussain, Cold spraying of titanium: A review of bonding mechanisms, microstructure and properties, Key Eng. Mater. 533 (2013) 53–90. doi:10.4028/www.scientific.net/KEM.533.53s.

[18] N.M. Melendez, A.G. McDonald, Development of WC-based metal matrix composite coatings using low-pressure cold gas dynamic spraying, Surf. Coatings Technol. 214 (2013) 101–109. doi:10.1016/j.surfcoat.2012.11.010.

[19] P.C. King, C. Busch, T. Kittel-Sherri, M. Jahedi, S. Gulizia, Interface melding in cold spray titanium particle impact, Surf. Coatings Technol. 239 (2014) 191–199. doi:10.1016/j.surfcoat.2013.11.039.

[20] M. Saleh, V. Luzin, K. Spencer, Analysis of the residual stress and bonding mechanism in the cold spray technique using experimental and numerical methods, Surf. Coatings Technol. 252 (2014) 15–28. doi:10.1016/j.surfcoat.2014.04.059.

[21] M.V. Vidaller, A. List, F. Gaertner, T. Klassen, S. Dosta, J.M. Guilemany, Single Impact Bonding of Cold Sprayed Ti-6Al-4V Powders on Different Substrates, J. Therm. Spray Technol. 24 (2015) 644–658. doi:10.1007/s11666-014-0200-4.

[22] F. Meng, H. Aydin, S. Yue, J. Song, The Effects of Contact Conditions on the Onset of Shear Instability in Cold-Spray, J. Therm. Spray Technol. 24 (2015) 711–719. doi:10.1007/s11666-015-0229-z.

[23] C. Lee, J. Kim, Microstructure of Kinetic Spray Coatings: A Review, J. Therm. Spray Technol. 24 (2015) 592–610. doi:10.1007/s11666-015-0223-5.

[24] O. Bielousova, J. Kocimski, R.G. Maev, I. Smurov, W. Scharff, V. Leshchynsky, Localisation of deformation in cold gas dynamic spraying, Surf. Eng. 32 (2016) 655–662. doi:10.1179/1743294415Y.0000000059.

[25] T.J. Watson, A. Nardi, A.T. Ernst, I. Cernatescu, B.A. Bedard, M. Aindow, Cold spray deposition of an icosahedral-phase-strengthened aluminum alloy coating, Surf. Coatings Technol. 324 (2017) 57–63. doi:10.1016/j.surfcoat.2017.05.049.

[26] A. Chaudhuri, Y. Raghupathy, D. Srinivasan, S. Suwas, C. Srivastava, Microstructural evolution of cold-sprayed Inconel 625 superalloy coatings on low alloy steel substrate, Acta Mater. 129 (2017) 11–25. doi:10.1016/j.actamat.2017.02.070.

[27] L. Zhu, T.-C. Jen, Y.-T. Pan, H.-S. Chen, Particle Bonding Mechanism in Cold Gas Dynamic Spray: A Three-Dimensional Approach, J. Therm. Spray Technol. 26 (2017) 1859–1873. doi:10.1007/s11666-017-0652-4.

[28] R. Kromer, Y. Danlos, E. Aubignat, C. Verdy, S. Costil, Coating deposition and adhesion enhancements by laser surface texturing—metallic particles on different classes of substrates in cold spraying process, Mater. Manuf. Process. 32 (2017) 1642–1652.

doi:10.1080/10426914.2017.1364750.

[29] W. Xie, A. Alizadeh-Dehkharghani, Q. Chen, V.K. Champagne, X. Wang, A.T. Nardi, S. Kooi, S. Müftü, J.-H. Lee, Dynamics and extreme plasticity of metallic microparticles in supersonic collisions, Sci. Rep. 7 (2017). doi:10.1038/s41598-017-05104-7.

[30] F. Meng, S. Yue, J. Song, Quantitative prediction of critical velocity and deposition efficiency in cold-spray: A finite-element study, Scr. Mater. (2015). doi:10.1016/j.scriptamat.2015.05.026.

[31] P.C. King, G. Bae, S.H. Zahiri, M. Jahedi, C. Lee, An Experimental and Finite Element Study of Cold Spray Copper Impact onto Two Aluminum Substrates, J. Therm. Spray Technol. 19 (2009) 620–634. doi:10.1007/s11666-009-9454-7.

[32] W.-Y. Li, C. Zhang, C.-J. Li, H. Liao, Modeling Aspects of High Velocity Impact of Particles in Cold Spraying by Explicit Finite Element Analysis, J. Therm. Spray Technol. 18 (2009) 921–933. doi:10.1007/s11666-009-9325-2.

[33] C.-J. Li, W.-Y. Li, H. Liao, Examination of the critical velocity for deposition of particles in cold spraying, J. Therm. Spray Technol. 15 (2006) 212–222. doi:10.1361/105996306X108093.

[34] L. Ajdelsztajn, A. Zúñiga, B. Jodoin, E.J. Lavernia, Cold gas dynamic spraying of a high temperature Al alloy, Surf. Coatings Technol. 201 (2006) 2109–2116. doi:10.1016/j.surfcoat.2005.06.001.

[35] R. Ghelichi, S. Bagherifard, M. Guagliano, M. Verani, Numerical simulation of cold spray coating, Surf. Coatings Technol. 205 (2011) 5294–5301. doi:10.1016/j.surfcoat.2011.05.038.

[36] Q. Wang, N. Birbilis, M.-X. Zhang, Interfacial structure between particles in an aluminum deposit produced by cold spray, Mater. Lett. 65 (2011) 1576–1578. doi:https://doi.org/10.1016/j.matlet.2011.03.035.

[37] M. Hassani-Gangaraj, D. Veysset, K.A. Nelson, C.A. Schuh, In-situ observations of single micro-particle impact bonding, Scr. Mater. 145 (2018) 9–13. doi:https://doi.org/10.1016/j.scriptamat.2017.09.042.

[38] M. Hassani-Gangaraj, D. Veysset, K.A. Nelson, C.A. Schuh, Melting can hinder impact-induced adhesion, Phys. Rev. Lett. 119 (2017) 175701.

[39] G.R. Johnson, W.H. Cook, Fracture characteristics of three metals subjected to various strains, strain rates, temperatures and pressures, Eng. Fract. Mech. 21 (1985) 31–48.

[40] M. Brünig, L. Driemeier, Numerical simulation of Taylor impact tests, Int. J. Plast. 23 (2007) 1979–2003. doi:10.1016/j.ijplas.2007.01.012.

[41] S. Rahmati, A. Ghaei, The use of particle/substrate material models in simulation of cold-gas dynamic-spray process, J. Therm. Spray Technol. 23 (2014) 530–540. doi:10.1007/s11666-013-0051-4.

[42] D.J. Benson, A multi-material Eulerian formulation for the efficient solution of impact and penetration problems, Comput. Mech. 15 (1995) 558–571. doi:10.1007/BF00350268.

[43] D.J. Benson, Computational methods in Lagrangian and Eulerian hydrocodes, Comput. Methods Appl. Mech. Eng. 99 (1992) 235–394. doi:10.1016/0045-7825(92)90042-I.

[44] M. Yu, W.-Y. Li, F.F. Wang, H.L. Liao, Finite Element Simulation of Impacting Behavior of Particles in Cold Spraying by Eulerian Approach, J. Therm. Spray Technol. 21 (2011) 745–752. doi:10.1007/s11666-011-9717-y.

[45] X.K. Suo, X.P. Guo, W.Y. Li, M.P. Planche, H.L. Liao, Investigation of Deposition Behavior of Cold-Sprayed Magnesium Coating, J. Therm. Spray Technol. 21 (2012) 831–837. doi:10.1007/s11666-012-9777-7.

[46] M. Yu, W.-Y. Li, F.F. Wang, X.K. Suo, H.L. Liao, Effect of particle and substrate preheating on particle deformation behavior in cold spraying, Surf. Coatings Technol. 220 (2013) 174–178. doi:10.1016/j.surfcoat.2012.04.081.

[47] W.Y. Li, M. Yu, F.F. Wang, S. Yin, H.L. Liao, A Generalized Critical Velocity Window Based on Material Property for Cold Spraying by Eulerian Method, J. Therm. Spray Technol. 23 (2013) 557–566. doi:10.1007/s11666-013-0023-8.

[48] F.F. Wang, W.Y. Li, M. Yu, H.L. Liao, Prediction of Critical Velocity During Cold Spraying Based on a Coupled Thermomechanical Eulerian Model, J. Therm. Spray Technol. 23 (2013) 60–67. doi:10.1007/s11666-013-0009-6.

[49] S. Yin, H.L. Liao, X.F. Wang, Euler based finite element analysis on high velocity impact behaviour in cold spraying, Surf. Eng. 30 (2014) 309–315. doi:10.1179/1743294413Y.0000000240.

[50] J. Xie, D. Nélias, H.W.-L. Berre, K. Ogawa, Y. Ichikawa, Simulation of the cold spray particle deposition process, J. Tribol. 137 (2015). doi:10.1115/1.4030257.

[51] A.G. Hanssen, Y. Girard, L. Olovsson, T. Berstad, M. Langseth, A numerical model for bird strike of aluminium foam-based sandwich panels, Int. J. Impact Eng. 32 (2006) 1127–1144. doi:10.1016/j.ijimpeng.2004.09.004.

[52] S. Heimbs, Computational methods for bird strike simulations: A review, Comput. Struct. 89 (2011) 2093–2112. doi:10.1016/j.compstruc.2011.08.007.

[53] M. Rein, Phenomena of liquid drop impact on solid and liquid surfaces, Fluid Dyn. Res. 12 (1993) 61–93. doi:10.1016/0169-5983(93)90106-K.

[54] J.E. Field, J.P. Dear, J.E. Ogren, The effects of target compliance on liquid drop impact, J. Appl. Phys. 65 (1989) 533. doi:10.1063/1.343136.

[55] D.E. Grady, The spall strength of condensed matter, J. Mech. Phys. Solids. 36 (1988) 353–384. doi:10.1016/0022-5096(88)90015-4.

[56] J.N. Johnson, Dynamic fracture and spallation in ductile solids, J. Appl. Phys. 52 (1981) 2812–2825. doi:10.1063/1.329011.

[57] M.A. Meyers, Dynamic Behavior of Materials, John Wiley & Sons, New York, 1994.

[58] P. Landau, S. Osovski, A. Venkert, V. Gärtnerová, D. Rittel, The genesis of adiabatic shear bands, Sci. Rep. 6 (2016) 37226. http://dx.doi.org/10.1038/srep37226.

[59] B. Crossland, Explosive welding of metals and its application, Oxford: Clarendon Press, 1982.

[60] J.M. Walsh, R.G. Shreffler, F.J. Willig, Limiting Conditions for Jet Formation in High Velocity

Collisions, J. Appl. Phys. 24 (1953) 349–359. doi:10.1063/1.1721278.

[61] L.E. Murr, C.-S. Niou, J.C. Sanchez, H.K. Shih, L. Duplessis, S. Pappu, L. Zernow, Comparison of beginning and ending microstructures in metal shaped charges as a means to explore mechanisms for plastic deformation at high rates, J. Mater. Sci. 30 (1995) 2747–2758. doi:10.1007/BF00349640.

[62] G. Birkhoff, D.P. MacDougall, E.M. Pugh, S.G. Taylor, Explosives with Lined Cavities, J. Appl. Phys. 19 (1948) 563–582. doi:10.1063/1.1698173.

[63] H.J. Melosh, C.P. Sonett, When worlds collide - Jetted vapor plumes and the moon's origin, in: N Orig. Moon; Proc. Conf. Kona, HI, Oct. 13-16, 1984 (A86-46974 22-91). Houston, TX, Lunar Planet. Inst., 1986: pp. 621–642.

[64] B.C. Johnson, T.J. Bowling, H.J. Melosh, Jetting during vertical impacts of spherical projectiles, Icarus. 238 (2014) 13–22. doi:http://dx.doi.org/10.1016/j.icarus.2014.05.003.

[65] F. Grignon, D. Benson, K.S. Vecchio, M.A. Meyers, Explosive welding of aluminum to aluminum: Analysis, computations and experiments, Int. J. Impact Eng. 30 (2004) 1333–1351. doi:10.1016/j.ijimpeng.2003.09.049.

[66] M. Hammerschmidt, H. Kreye, Microstructure and Bonding Mechanism in Explosive Welding, in: Shock Waves High-Strain- Rate Phenom. Met., 1981: pp. 961–973.

[67] J. Vlcek, L. Gimeno, H. Huber, E. Lugscheider, A systematic approach to material eligibility for the cold-spray process, J. Therm. Spray Technol. 14 (2005) 125–133. doi:10.1361/10599630522738.

[68] J.E. Field, J.J. Camus, M. Tinguely, D. Obreschkow, M. Farhat, Cavitation in impacted drops and jets and the effect on erosion damage thresholds, Wear. 290–291 (2012) 154–160. doi:10.1016/j.wear.2012.03.006.

[69] M. Hahn, C. Weddeling, G. Taber, A. Vivek, G.S. Daehn, A.E. Tekkaya, Vaporizing foil actuator welding as a competing technology to magnetic pulse welding, J. Mater. Process. Technol. 230 (2016) 8–20. doi:https://doi.org/10.1016/j.jmatprotec.2015.11.010.

[70] G.R. Osinski, E. Pierazzo, Impact Cratering: Processes and Products, Wiley, 2012. https://books.google.com/books?id=3Vzky11ZR3UC.

[71] E. Orowan, Fracture and strength of solids, Reports Prog. Phys. 12 (1949) 185–232. doi:10.1088/0034-4885/12/1/309.

[72] T. Antoun, L. Seaman, D.R. Curran, G.I. Kanel, S. V Razorenov, A. V Utkin, Spall Fracture, Springer New York, 2006. https://books.google.com/books?id=RdARBwAAQBAJ.

[73] Dassault Systemes, ABAQUS 6.14-3 User's manual, 2014.

[74] C. Kittel, Introduction to Solid State Physics, John Wiley & Sons, New York, 2004.